

Pontificia Universidad Católica del Perú

Escuela de Posgrado



PONTIFICIA
UNIVERSIDAD
CATÓLICA
DEL PERÚ

Tesis:

**“Búsqueda de correlaciones de rayos gamma con nuevas
fuentes de radio astrofísicas”**

**Para obtener el grado de
Magíster en Física**

Presentada por

Sergio André Best Reyes

Asesor:

Dr. José Luis Bazo Alba

Lima–Perú, 2019

Agradecimientos

Quisiera agradecer a Concytec-Fondecyt (Convenio 233-2015-2) por la beca que me permitió estudiar esta maestría, sin la cual esta tesis no existiría; a mi asesor, el Profesor José Bazo por su apoyo, dedicación al proyecto y enseñarme todas las herramientas y técnicas necesarias para llevar a cabo este proyecto; y a mis padres, ya que de no ser por todos sus años de dedicación y esfuerzo no habría podido estudiar la carrera de física.



Resumen

In this work we study two newly discovered classes of radio sources: the highly energetic, short-lived events, known as Fast Radio Bursts (FRBs), and a new category of compact sources known as Fanaroff-Riley type 0 radio galaxies (FROs). Due to a possible catastrophic event origin for the FRBs and a previous correlation found with an FRO in the Γ -rays spectrum, it is possible that these radio sources could also emit high energy photons in the Fermi-LAT satellite energy range (20 MeV - 300 GeV). Here we present an exhaustive time-dependent and spatial search of all up-to-date observed FRBs and FROs, respectively. We perform a likelihood analysis of the radio sources by modeling the excess flux of gamma rays with a varying index power law function using data from Fermi-LAT and the 3FGL catalog. No correlations with more than 5σ were found. Two FRBs and one FRO with more than 4σ were further analyzed. However, the significance from these sources is most likely due to nearby blazars. Therefore, upper limits for all sources are calculated.

En este trabajo, estudiamos dos nuevas clases de fuentes de radio recientemente descubiertas: un tipo de fuente altamente energética y de corta duración conocidas como Fast Radio Bursts (FRBs) y la nueva categoría de fuentes compactas conocidas como radio galaxias Fanaroff-Riley tipo 0 (FROs). Debido a un posible origen de evento catastrófico para los FRBs y una previa correlación encontrada de un FRO con rayos gamma, es posible que estas fuentes de radio emitan también fotones de muy alta energía en el rango que mide el satélite Fermi-LAT (20 MeV - 300 GeV). Aquí presentamos una búsqueda temporal y espacial exhaustiva de todos los FRBs y FROs observados y documentados en los catálogos presentes. Realizamos un análisis de verosimilitud modelando el exceso del flujo de rayos gamma con índice variable de una ley de potencias con data de Fermi-LAT y el catálogo 3FGL. Dos FRBs y un FRO con más de 4 sigmas fueron analizados más a fondo. Sin embargo, la significancia de estas fuentes es mayormente debido a blazares cercanos. Por tanto, límites superiores en el flujo para todas las fuentes son presentados.

Search for gamma-ray counterparts of newly discovered radio astrophysical sources

SERGIO BEST¹ AND JOSÉ BAZO¹

¹*Sección Física, Departamento de Ciencias, Pontificia Universidad Católica del Perú, Av. Universitaria 1801, Lima 32, Perú*

ABSTRACT

In this paper we study two newly discovered classes of radio sources: the highly energetic, short-lived events, known as Fast Radio Bursts (FRBs), and a new category of compact sources known as Fanaroff-Riley type 0 radio galaxies (FR0s). Due to a possible catastrophic event origin for the FRBs and a previous correlation found with an FR0 in the γ -ray spectrum, it is possible that these radio sources could also emit high energy photons in the Fermi-LAT satellite energy range (20 MeV - 300 GeV). Here we present an exhaustive time-dependent and spatial search of all up-to-date observed FRBs and FR0s, respectively. We perform a likelihood analysis of the radio sources by modeling the excess flux of gamma rays with a varying index power law function using data from Fermi-LAT and the 3FGL catalog. No correlations with more than 5σ were found. Two FRBs and one FR0 with more than 4σ were further analyzed. However, the significance from these sources is most likely due to nearby blazars. Therefore, upper limits for all sources are calculated.

Keywords: Fermi-LAT, Fast Radio Burst, Fanaroff-Riley type 0, Radio Galaxies, γ -rays correlation

1. INTRODUCTION

As more satellite and ground-based telescopes start to gather data covering different parts of the electromagnetic spectrum, new windows of opportunity for astronomy are opened. The possibility to observe the same source through different wavelengths can give us valuable information about the processes occurring inside our target. Although Fast Radio Bursts (FRBs) and Fanaroff-Riley type 0 galaxies (FR0) were first discovered in the radio spectrum, it is possible that these radio sources could also emit high energy photons in the Fermi-LAT satellite energy range (20 MeV - 300 GeV) (Margalit et al. 2018). Here we search for such correlations that could help us to better understand their origin and the engine driving their photon production.

Fast Radio Bursts (FRBs) are very energetic, short lived (milliseconds), radio intense events which are thought to be extragalactic in origin due to their spatial distribution and their dispersion measure (DM) (Lorimer et al. 2007). Up to date, only one FRB (FRB121102) has been correlated with a known galaxy (Chatterjee et al. 2017). As these radio emissions already release a great amount of energy, if they were to emit gamma-rays as well, they could be candidates to most energetic events of the universe while providing important clues as to their origin. Possible origins for these gamma-ray emission signals are powerful events such as gamma-ray bursts, magnetar giant flares, neutron star merging (Margalit et al. 2018), primordial black hole merging (Deng et al. 2018), etc. These emissions could occur before or after the radio emission itself and so we look for correlations before and after the arrival time of the radio signal. Some FRBs are found during searches for other astronomical events such as the Parkes Telescope search for Pulsars, which could make them correlate with these sources like FRB180309 and FRB180311 (Osłowski, S. 2018).

The second source analyzed in this work are the Fanaroff-Riley type 0 radio galaxies. Fanaroff-Riley original classification (Fanaroff et al. 1974) divides compact radio galaxies in type I (low intensity, with the bulk of the radio emissions coming from the core) and type II (high intensity with luminosity increasing in the lobes). Recently a new category, called type 0 (Baldi et al. 2015), has been added. FR0 galaxies are similar to type I except for a large deficit of extended radio structures. These are not believed to be FRIs seen from another angle due to FR0s being much more common (Baldi et al. 2017). The study of FR0s in other wavelengths is crucial to better understand

the engine driving the emission of these radio galaxies and to further differentiate them from FRIs. In addition, one correlation of an FR0 with gamma rays has already been found (Grandi et al. 2015).

In Section 2 of this paper we briefly describe the historical radio observations leading to the discovery of this sources. Next, in Section 3 we detail the binned likelihood analysis using Fermi-LAT data for both sources. In Section 4 we present the results of these analyses including the optimal set of parameters for the model of each source which maximizes the TS (Test Statistic) of the excess gamma-ray flux. Detailed information and further analysis of the sources with the highest TS (≥ 16) are also presented. The significance of these correlations will be discussed as to offer a possible explanation.

2. RADIO SOURCES OBSERVATIONS

The sources mentioned in this paper (both FRBs and FR0s) were both first detected in the radio spectrum. The first FRB was discovered in 2007 by Lorimer (Lorimer et al. 2007), but only recently new telescopes covering this range of frequencies have increased the number of detected FRBs. Now, with telescopes like the CHIME, we expect to see dozens of FRBs each year, proving they are not isolated events.

The FR0 class was added in 2015 to accommodate an increasingly number of sources which did not match well with the FRI class and which now constitute the most numerous class in the Fanaroff-Riley classification.

We focus our attention for the FR0s (a very numerous source) in a subset of 108 sources catalogued (Baldi et al. 2017) as part of the SSDS survey and in the case of FRBs, 62 events which had been detected by many telescopes (e.g. CHIME, ASKAP, Parkes, etc) (Petroff et al. 2016) at the time of the analysis. A map in galactic coordinates of both types of sources can be seen in Fig. 1, showing their extragalactic origin.

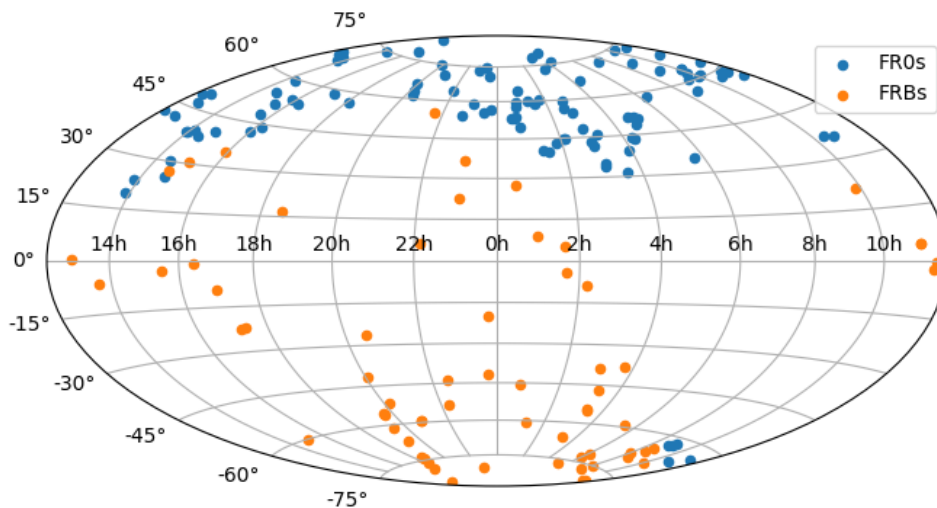


Figure 1. Sky map in galactic coordinates of all sources, both FRBs and FR0s, studied in this paper. The spatial distribution of FRBs suggests their extragalactic origin.

There have been previous attempts to observe these sources in other wavelengths such as X-rays (Scholz et al. 2017) and γ -rays (Shao-Qiang Xi et al. 2017). Nevertheless, the search (temporal in the case of FRBs and spatial in the case of FR0s) presented in this paper is more exhaustive, in the sense that it is applied to all sources listed in the available catalogs mentioned above.

3. FERMI-LAT DATA ANALYSIS

The LAT, Large Area Telescope, on board of the Fermi Telescope satellite, is an imaging gamma-ray detector that uses pair production to detect both energy and momentum of high energy incident photons (20 MeV - 300 GeV). It covers at any given moment around 20% of the sky with a high resolution of arcminutes and has been collecting data since 2008 (Atwood et al. 2009).

We extracted the photon data files and spacecraft history from the LAT server using the time and coordinates provided by the FRB catalog (Petroff et al. 2016) (62 sources) and the FR0 catalog (Baldi et al. 2017) (108 sources)

with an Astroquery (Ginsburg, A. 2019) script. In the case of FRBs, we extracted data 25 hours around the radio event (1 day + 1 hour so the event is included in the central time bin) and 15 days around the radio event for a second analysis. For FR0s we took the most recent six months of data available at the moment of starting the analysis (from 3-9-18 to 9-9-18). Both included photons from 100 MeV to 300 GeV. For both studies we used Fermi LAT Pass 8 data with Fermi Science Tools v11r5p3 and Enrico (Sanchez & Deil 2013), a data analysis package for the Fermi ScienceTools.

To reduce contamination from Earth's limb emission we used a maximum zenith angle of 90° and took events only when the spacecraft was operating correctly ([DAT && QUALITY] == 1). We then selected for events corresponding to all SOURCE class events (evclass=128 and evtype=3) and used the IRFs (Instrument Response Function): P8R2_SOURCE_V6. We took a ROI (region of interest) of 10° and set the background sources using the 3FGL catalog. For convergence purposes, all source's index were fixed to their catalog value and only normalization was left free to vary. We used gll_iem_v06 to model the galactic background and iso_P8R2_SOURCE_V6_v06 for the extragalactic background.

For FRBs as well as for FR0s, we modeled the filtered data using a Power Law (Eq. 1) with a varying Γ index from 1.75 to 3.0 in steps of 0.25, with a fixed energy scale E_0 of 100 MeV for the binned likelihood analysis.

$$\frac{dN}{dE} = N_0 \left(\frac{E}{E_0} \right)^{-\Gamma} \quad (1)$$

We applied a time-dependent analysis to the FRBs using two time scales. First, for a precise search the 25 hour photon data was divided in bins of one hour and the binned likelihood was applied to each bin. In the second case, for a broader study around 15 days of the time of the FRB, we used a binning of one day for better statistics.

A spatial search, varying the source location by 0.1° in a grid of $1.1^\circ \times 1.1^\circ$, was applied to the FR0s. For each case we get a TS (i.e. likelihood-ratio test) value defined by:

$$TS = -2 \log \left(\frac{L|\theta_0}{L|\theta_{ML}} \right) \quad (2)$$

where L represents the likelihood given θ_0 , the set of parameters representing the null hypothesis, and θ_{ML} , the most likely value of the set of parameter given the data. The square root of the TS can be treated as the detection significance since we are fitting over only one parameter.

Due to the large number of sources to be studied we did the analysis described before as a preliminary one to select the most promising sources. Then, more detailed tests were used for the sources with higher TS (≥ 16) including light curves and spectral energy distributions for the FRBs, as well as using an exponential cutoff model, given in Eq. 3. In this case, we looped over both $\Gamma_{[1,2]}$ indices, the energy cutoff, E_C , and left the normalization, N_0 , to vary freely. In addition, we applied a larger TS spatial map for FR0s (21 pixels with the same 0.1° resolution).

$$\frac{dN}{dE} = N_0 \left(\frac{E}{E_0} \right)^{-\Gamma_1} \exp \left(- \left(\frac{E}{E_C} \right)^{-\Gamma_2} \right) \quad (3)$$

4. RESULTS

The results of our search can be found summarized in the Appendix in Table 2 and Table 3, for FRBs and FR0s, respectively. We present for each source the set of parameters which maximizes the TS, including the Γ index of the fitted power law (see Eq. 1). In addition, in the case of FRBs, the time from the radio event is given, corresponding to the highest TS from either one hour or one day binning. For FR0s the distance from the detected radio source, in right ascension and declination, is shown. The resulting maximum TS is also presented as sky maps in galactic coordinates in Fig. 2 and Fig. 3, for FRBs and FR0s, respectively.

In every case, we found a TS lower than 25 (approximately 5σ), so we calculated the flux Upper Limit with a 95% confidence level, also shown in Tables 2 and 3. There we highlight the sources and parameters with a $TS \geq 16$ which corresponds to roughly 4σ . There are only two FRBs and one FR0 satisfying this criteria: FRB130628, FRB170712 and FR0 SDSS_J101806.67+000559.7. Given that these are the most promising sources, we give more details about them.

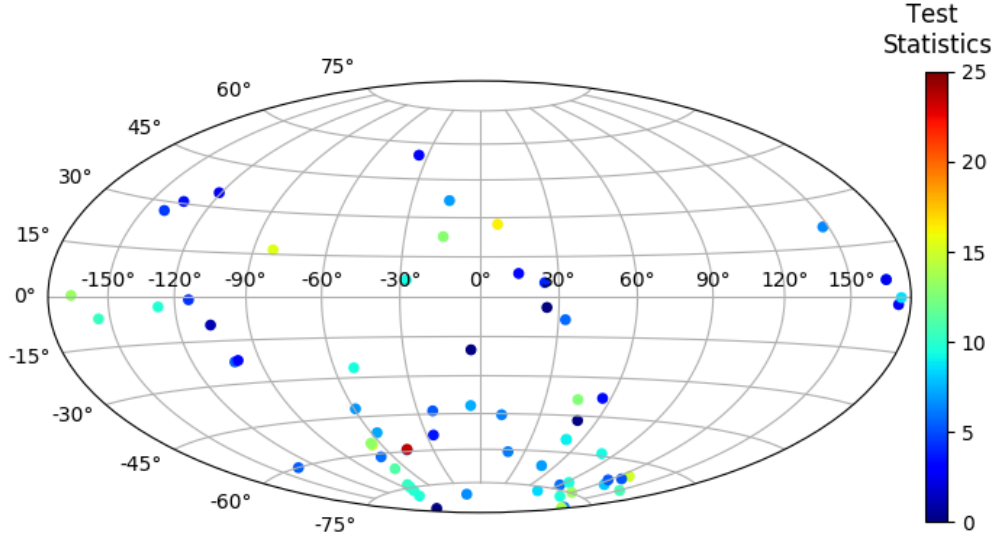


Figure 2. Sky map in galactic coordinates of 62 analyzed FRBs showing the maximum TS found according to the color scale. The TS corresponds to the best combination of time binning, time from the FRB event and Γ index of the power law. The exact values are listed in Table 2.

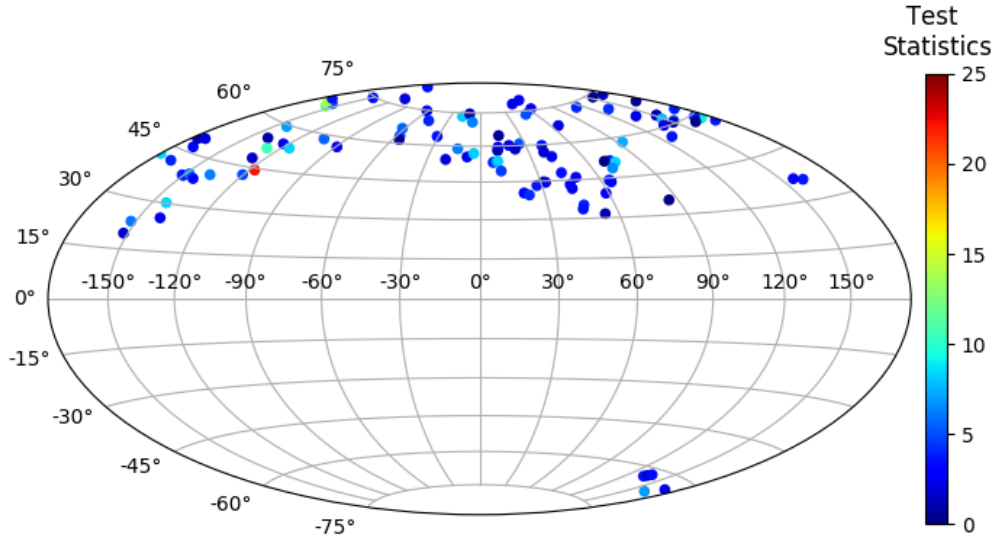


Figure 3. Sky map in galactic coordinates of 108 analyzed FR0s showing the maximum TS found according to the color scale. The TS corresponds to the best combination of the source's position in a spatial grid and Γ index of the power law. The exact values are listed in Table 3.

In Fig. 4 we show the light curves of these two FRBs presenting flux upper limits. The upper limits are calculated using the Γ index that gave the highest TS in one of the time bins. The markers' color represents the value of the TS. No significant possible enhancement (i.e. flare) around the time of the event is observed.

In addition, we calculated the source's SED (spectral energy distribution). Since FRB130628 only has upper limits in its SED we are not showing it. We present the SED of FRB170712 in Fig. 5. The photon counts are in the lower energy range of the spectrum. The only nearby source is 3FGL J2141.6-6412, a blazar more than 2° away from the FRB. However, the measured flux is within 2σ of the 3FGL catalogued source. Nevertheless, this is the most promising source of our search. We performed the same analysis for FRB170712 using an exponential cutoff (Eq. 3) with $\Gamma_2 = 1, 2$ and $E_C = 100, 500$. We get a higher TS (23.75) and a flux upper limit of $2.33e-06$ ph cm $^{-2}$ s $^{-1}$ in the same time bin as before (8 hours after the radio event) with the same $\Gamma_1 = 3.0$ index using $\Gamma_2 = 1$ and $E_C = 500$.

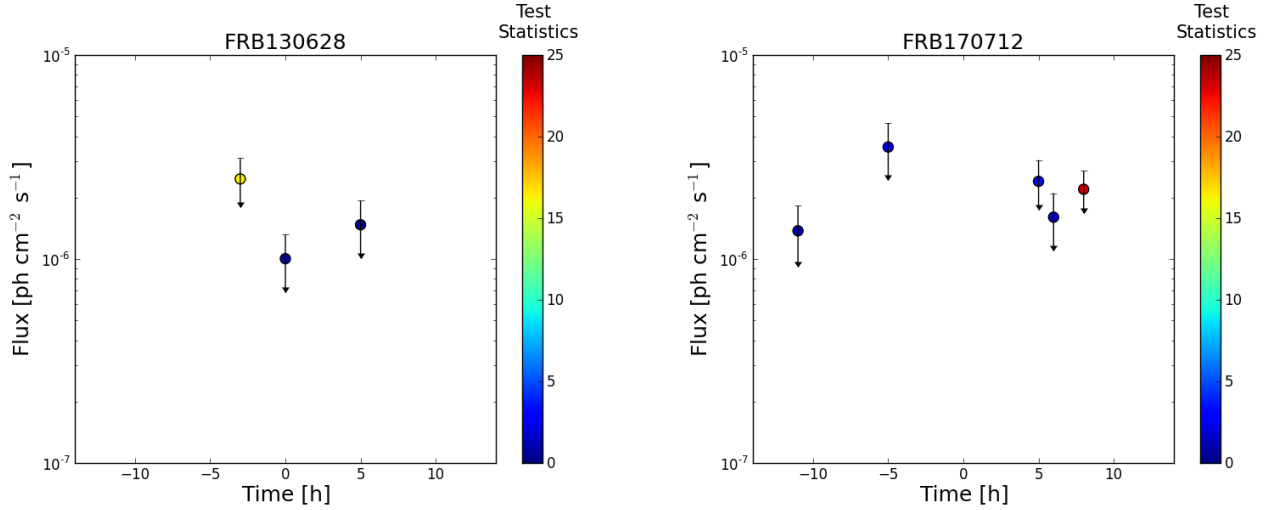


Figure 4. Light curves of the two most significant FRBs showing flux upper limits. The time axis is centered at the radio event’s detection time using a 1 hour bin. The Γ index corresponds to highest TS found and the color represents the TS. The points that do not appear are due to the TS being negative or the non-convergence of the fit. Left: FRB130628, max. TS = 16.35 ($\Gamma = 1.75$). Right: FRB170712, max. TS = 23.48 ($\Gamma = 3.0$).

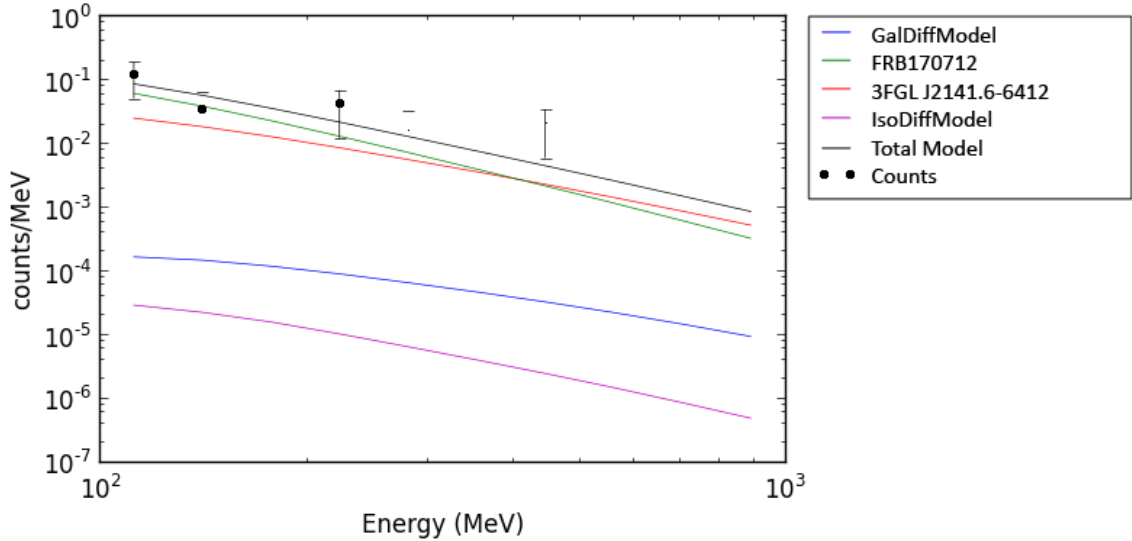


Figure 5. Spectral energy distribution of FRB170712 using the Γ index ($\Gamma = 3$) and time bin (one hour) which corresponds to the maximum TS. Points represent the data from Fermi. The black line is the total model (i.e. the sum of the individual fits), the green line represents the studied FRB and the red line corresponds to the source 3FGL J2141.6-6412, which is a blazar. The blue and magenta lines represent the galactic diffuse emission model and the extragalactic isotropic diffuse emission model, respectively.

Then we analyzed the only FR0 (i.e. SDSS_J101806.67+000559.7) with resulting $TS \geq 16$. In Fig. 6 we show maps of the TS and flux upper limits using a spatial grid of 11 by 11 pixels. The source position was varied from pixel to pixel by 0.1° starting from the position of the FR0, as described in the FR0 catalog. We show the maps corresponding to the Γ index that gave the best TS.

We then contrasted the areas of high TS with known sources from the 3FGL catalog. The FR0 under study, with equatorial coordinates (154.53, 0.09), has 5 sources closer than 5° according to the 3FGL catalog, shown in Table 1.

Table 1. Sources closer than 5° to SDSS_J101806.67+000559.7

Source Name	R.A. ($^\circ$)	Dec. ($^\circ$)	Distance ($^\circ$)
3FGL J1007.8+0026	151.964	0.442	2.58
3FGL J1010.8-0158	152.713	-1.976	2.75
3FGL J1022.8-0113	155.704	-1.224	1.77
3FGL J1024.8+0105	156.224	1.096	1.96
3FGL J1028.5-0235	157.144	-2.585	3.74

NOTE—Column description: (1) Source name; (2) (3) Right ascension (declination) in equatorial coordinates; (4) distance to FR0.

Of these sources, 3FGL J1024.8+0105 (a blazar) is in the direction of the increasing TS according to Fig. 6. This was further corroborated by an extended TS map using 21 by 21 pixels and a 5° count map surrounding the FR0's position. Therefore, the possible FR0 4σ excess is actually due to the nearby blazar.

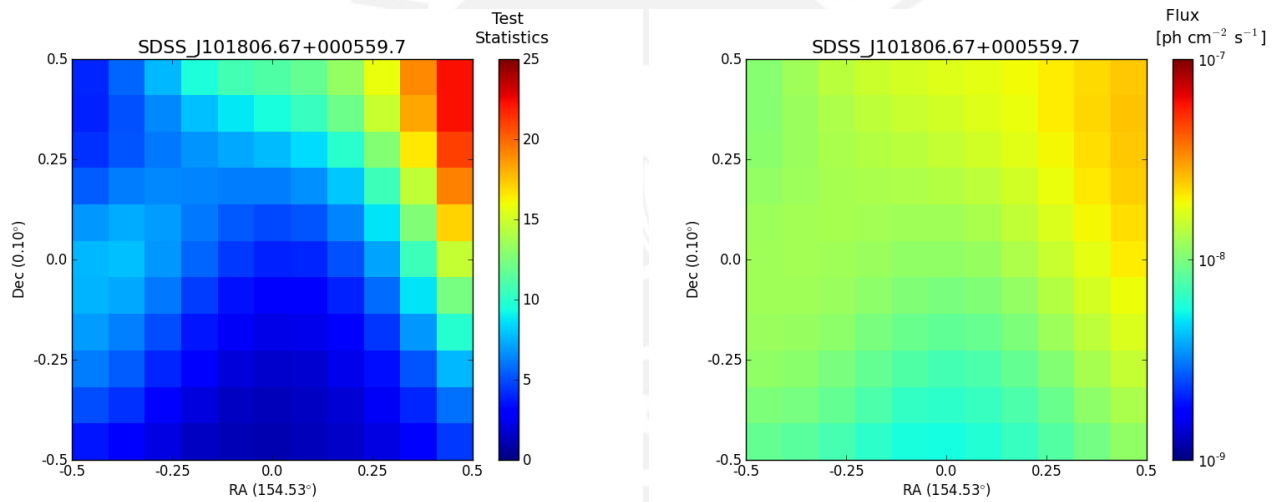


Figure 6. Spatial grid maps of Left: Test statistic, Right: Flux upper limits. Each pixel in the map represents a displacement of 0.1° from the detected central position of the source SDSS_J101806.67+000559.7 in right ascension and declination. The results correspond to the Γ index that gave the maximum TS ($\Gamma = 2.5$).

5. CONCLUSIONS

We analyzed 62 FRBs and 108 FR0s, extragalactic sources discovered in radio, searching for a correlation with Fermi-LAT gamma ray data. We performed time-dependent (FRB) and spatial (FR0) searches using a binned likelihood analysis fixing the Γ index of a power law that describes their flux, only letting one parameter (i.e. normalization) vary.

From these sources, only three (two FRBs and one FR0) had a Test Statistic higher than 16 (roughly 4σ) but non of them reached 5σ . From the two FRBs we discarded FRB130628 due to bad fitting. Only FRB170712 seems to be promising, even if a not so close blazar could explain its SED. The correlation with the FR0 was found to be also due to a nearby blazar. Therefore we have calculated flux upper limits for all sources.

This work can be improved using the soon to be released 4FGL catalog, which will include data from 8 years of Fermi-LAT, and can be updated as new sources are discovered.

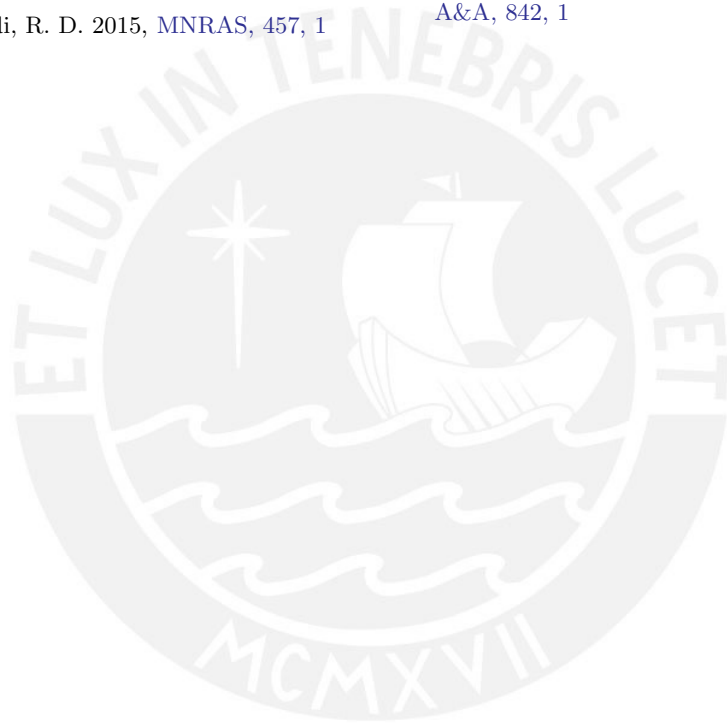
ACKNOWLEDGMENTS

S.B. acknowledges support from the Peruvian National Science and Technology Council scholarship under grant CONCYTEC-FONDECyT 233-2915-2. J.B. acknowledges funding by the Dirección de Gestión de la Investigación at PUCP under grant No. DGI-2017-3-0019.



REFERENCES

- Atwood, W. B., Abdo, A. A., Ackermann, M., et al. 2009, *ApJ*, 697, 1071
- Baldi, R. D., Capetti, A., & Giovannini, G. 2015, *AN*, 337, Issue 1-2
- Baldi, R. D., Capetti, A., & Massaro, F. 2017, *A&A*609, A1
- Chatterjee, S., Law, C. J., Wharton, R. S., et al. 2017, *Nature*, 337, 541, 58-61
- Deng, C. M., Cai, Y., Wu, X. F., Liang, E. W. 2018, *PhRvD*, 98, 123016
- Fanaroff B. L., & Riley J. M., 1974, *MNRAS*, 167, 31P
- Ginsburg, A., Astroquery 2019, <https://astroquery.readthedocs.io/en/latest/>
- Grandi, P., Capetti, A., Baldi, R. D. 2015, *MNRAS*, 457, 1
- Lorimer, D. R., Bailes, M., McLaughlin, M. A., Narkevic, D. J., & Crawford, F. 2007, *Sci*, 318, 5851
- Margalit, B., Metzger, B. D., Berger, E., et al. 2018, *MNRAS*, 481, 2
- Osowski, S. 2018, <http://www.astronomerstelegam.org/?read=11396>
- Petroff, E., Barr, E. D., Jameson, A., et al. 2016, *PASA*, 33, e045, <http://frbcat.org>
- Sanchez, D., Deil, C., Enrico 2013, <https://enrico.readthedocs.io/en/latest/>
- Scholz, P., Bogdanov, S., Hessels, J. W., et al. 2017, *A&A*, 846, 1
- Xi, S. Q., Tam, P. H. T., Peng, F. K., Wang, X. Y. 2017, *A&A*, 842, 1



APPENDIX

Table 2. Fast Radio Bursts: summary of the parameters for the maximum TS.

Source Name	Gamma Index (Γ)	Time from event (h)	Flux (10^{-6}) ($\text{ph cm}^{-2} \text{s}^{-1}$)	Test Statistic
FRB090625	3.0	4d 0h	0.38	6.76
FRB110214	2.75	-1d 0h	0.28	5.42
FRB110220	1.75	0d 12h	4.85	11.18
FRB110523	3.0	0d 10h	2.92	9.07
FRB110626	1.75	1d 0h	0.24	3.35
FRB110703	3.0	0d 10h	2.60	7.41
FRB120127	3.0	-3d 0h	0.75	9.30
FRB121002	2.25	-0d 5h	2.01	6.94
FRB121102	3.0	0d 6h	12.60	9.55
FRB130626	3.0	0d 5h	4.81	8.61
FRB130628	1.75	-0d 3h	2.47	16.35
FRB130729	3.0	-2d 0h	0.55	3.43
FRB131104	1.75	1d 0h	0.14	3.09
FRB140514	3.0	-3d 0h	0.47	3.06
FRB141113	1.75	0d 0h	10.00	10.20
FRB150215	2.75	0d 0h	8.64	13.37
FRB150418	2.25	0d 4h	9.96	3.93
FRB150610	3.0	-5d 0h	0.52	9.83
FRB150807	3.0	0d 8h	3.22	15.44
FRB151018	1.75	-0d 9h	0.65	3.56
FRB151206	3.0	7d 0h	0.74	3.18
FRB151230	3.0	1d 0h	0.40	5.68
FRB160102	1.75	-0d 7h	0.67	2.60
FRB160317	2.75	-2d 0h	1.18	6.18
FRB160410	3.0	-0d 1h	2.02	4.39
FRB160608	2.0	-7d 0h	0.19	4.56
FRB160920	3.0	-2d 0h	0.44	1.16
FRB170107	3.0	0d 6h	2.50	2.38
FRB170416	3.0	-0d 10h	2.90	5.34
FRB170428	3.0	0d 9h	2.11	5.81
FRB170606	1.75	0d 0h	7.21	10.34
FRB170707	3.0	-6d 0h	0.35	6.56
FRB170712	3.0	0d 8h	2.20	23.48
FRB170827	1.75	0d 5h	1.25	13.17
FRB170906	3.0	0d 4h	3.18	7.28

Table 2 continued on next page

Table 2 (*continued*)

Source Name	Gamma Index (Γ)	Time from event (h)	Flux (10^{-6}) ($\text{ph cm}^{-2} \text{s}^{-1}$)	Test Statistic
FRB170922	2.5	-0d 1h	4.52	13.78
FRB171003	2.0	6d 0h	0.50	12.68
FRB171004	3.0	-0d 5h	4.77	9.76
FRB171019	2.25	0d 0h	2.60	13.51
FRB171020	3.0	-0d 4h	2.19	10.65
FRB171116	1.75	0d 10h	1.32	6.15
FRB171209	2.0	-0d 1h	5.94	8.46
FRB171213	2.0	0d 4h	1.19	9.34
FRB171216	3.0	0d 10h	2.22	9.49
FRB180110	2.75	-0d 5h	1.90	6.98
FRB180119	2.5	6d 0h	0.36	9.68
FRB180128.0	2.25	-5d 0h	0.29	5.82
FRB180128.2	3.0	-7d 0h	0.55	8.03
FRB180130	2.5	-0d 10h	1.73	14.44
FRB180131	3.0	3d 0h	0.45	9.95
FRB180212	2.75	0d 12h	4.54	9.45
FRB180301	2.25	-0d 5h	3.01	5.20
FRB180309	1.75	-4d 0h	0.21	10.39
FRB180311	3.0	0d 2h	1.82	6.31
FRB180315	1.75	-5d 0h	0.14	5.29
FRB180525	1.75	-2d 0h	0.17	6.62
FRB180528	2.75	-0d 11h	6.15	15.10
FRB180714	3.0	7d 0h	3.64	5.40
FRB180725A	3.0	7d 0h	0.37	3.24
FRB180923	1.75	5d 0h	0.62	6.49
FRB181016	1.75	0d 10h	2.26	6.99
FRB181017	1.75	-0d 8h	1.23	12.87

NOTE—Column description: (1) Source name; (2) Γ index of the power law which gave the maximum TS; (3) Time difference between the radio event time specified in the FRB catalog and the central time of the bin; (4) Flux upper limit (95% confidence level) corresponding to the maximum TS found in photons per centimeter square per second; (5) Maximum TS found for this source.

Table 3. Fanaroff-Riley type 0 radio galaxies: summary of the parameters for the maximum TS.

Source Name	Right Ascension distance (°)	Declination distance (°)	Gamma Index (Γ)	Flux (10^{-9}) (ph cm $^{-2}$ s $^{-1}$)	Test Statistic
SDSS_J010852.48-003919.4	-0.1	-0.5	1.75	1.03	3.64
SDSS_J011204.61-001442.4	-0.2	0.1	1.75	0.38	1.85
SDSS_J011515.78+001248.4	0.4	-0.5	3.0	11.89	3.34
SDSS_J015127.10-083019.3	0.5	0.0	2.5	9.68	6.99
SDSS_J020835.81-083754.8	-0.1	0.0	1.75	0.52	2.40
SDSS_J075354.98+130916.5	0.4	0.4	3.0	10.07	1.68
SDSS_J080716.58+145703.3	0.1	0.3	1.75	1.19	6.10
SDSS_J083158.49+562052.3	0.2	0.3	1.75	0.55	3.66
SDSS_J083511.98+051829.2	0.2	-0.5	1.75	0.59	2.38
SDSS_J084102.73+595610.5	-0.5	-0.5	1.75	1.09	3.05
SDSS_J084701.88+100106.6	-0.2	0.2	1.75	1.64	8.37
SDSS_J090652.79+412429.7	-0.4	0.0	1.75	1.63	8.31
SDSS_J090734.91+325722.9	0.5	0.5	2.25	5.86	3.94
SDSS_J090937.44+192808.2	-0.4	0.0	1.75	0.74	4.21
SDSS_J091039.92+184147.6	0.1	-0.4	1.75	1.13	3.79
SDSS_J091601.78+173523.3	0.5	0.5	3.0	19.27	6.11
SDSS_J091754.25+133145.5	0.3	0.4	2.5	7.38	3.11
SDSS_J093003.56+341325.3	-0.5	-0.1	2.0	2.21	2.97
SDSS_J093346.08+100909.0	0.5	0.2	2.0	4.12	6.32
SDSS_J093938.62+385358.6	0.5	-0.3	2.5	3.54	1.08
SDSS_J094319.15+361452.1	-0.4	-0.2	1.75	0.44	2.07
SDSS_J100549.83+003800.0	-0.1	0.2	1.75	0.94	4.94
SDSS_J101329.65+075415.6	-0.5	0.2	1.75	0.38	1.57
SDSS_J101806.67+000559.7	-0.5	-0.4	2.5	0.03	22.35
SDSS_J102403.28+420629.8	0.2	-0.5	2.25	3.52	3.57
SDSS_J102511.50+171519.9	0.2	0.2	2.25	1.86	0.91
SDSS_J102544.22+102230.4	-0.2	-0.5	2.5	13.26	10.70
SDSS_J103719.33+433515.3	0.0	-0.5	2.75	13.38	9.08
SDSS_J103952.47+205049.3	0.1	0.2	3.0	17.26	7.11
SDSS_J104028.37+091057.1	0.4	0.5	1.75	0.69	2.42
SDSS_J104403.68+435412.0	0.3	0.0	2.25	3.12	3.57
SDSS_J104811.90+045954.8	0.0	0.5	2.25	6.83	8.29
SDSS_J104852.92+480314.8	0.5	0.1	2.75	1.17	0.10
SDSS_J105731.16+405646.1	-0.1	-0.2	1.75	0.87	3.75
SDSS_J111113.18+284147.0	0.4	-0.4	2.0	5.53	12.19
SDSS_J111622.70+291508.2	-0.5	-0.2	2.5	7.04	4.94
SDSS_J111700.10+323550.9	0.2	-0.1	2.25	9.50	13.98
SDSS_J112029.23+040742.1	0.3	-0.3	1.75	1.15	5.62

Table 3 continued on next page

Table 3 (continued)

Source Name	Right Ascension distance ($^{\circ}$)	Declination distance ($^{\circ}$)	Gamma Index (Γ)	Flux (10^{-9}) ($\text{ph cm}^{-2} \text{s}^{-1}$)	Test Statistic
SDSS_J112039.95+504938.2	-0.5	0.5	1.75	1.15	5.58
SDSS_J112256.47+340641.3	0.2	0.3	1.75	0.99	3.52
SDSS_J112625.19+520503.5	-0.5	-0.2	1.75	0.29	0.94
SDSS_J112727.52+400409.4	-0.2	-0.1	2.0	0.56	0.45
SDSS_J113446.55+485721.9	-0.1	-0.4	2.5	3.01	1.46
SDSS_J113449.29+490439.4	-0.1	-0.3	2.5	2.75	1.29
SDSS_J113637.14+510008.5	0.2	0.5	1.75	1.50	7.74
SDSS_J114230.94-021505.3	0.4	-0.3	1.75	0.65	2.43
SDSS_J114232.84+262919.9	0.5	0.3	2.5	6.23	3.55
SDSS_J114804.60+372638.0	-0.5	0.0	1.75	0.54	1.30
SDSS_J115531.39+545200.4	0.5	-0.5	1.75	0.48	2.28
SDSS_J120551.46+203119.0	0.2	-0.4	1.75	0.59	2.02
SDSS_J120607.81+400902.6	0.5	-0.4	3.0	2.72	0.26
SDSS_J121329.27+504429.4	-0.5	-0.5	2.25	3.15	2.44
SDSS_J121951.65+282521.3	0.1	-0.1	1.75	0.66	3.50
SDSS_J122421.31+600641.2	-0.5	-0.5	3.0	8.34	3.55
SDSS_J123011.85+470022.7	-0.2	0.2	1.75	0.65	4.21
SDSS_J124318.73+033300.6	0.4	0.5	3.0	16.32	5.55
SDSS_J124633.75+115347.8	-0.2	0.1	1.75	0.60	2.15
SDSS_J125027.42+001345.6	0.3	-0.5	1.75	0.88	4.97
SDSS_J125409.12-011527.1	-0.3	-0.4	2.5	3.01	0.81
SDSS_J130404.99+075428.4	-0.1	-0.5	1.75	1.05	4.07
SDSS_J130837.91+434415.1	0.0	0.0	1.75	0.87	4.08
SDSS_J133042.51+323249.0	0.5	0.5	2.25	3.35	3.05
SDSS_J133455.94+134431.7	0.3	-0.3	2.0	3.44	8.11
SDSS_J133621.18+031951.0	0.2	-0.4	1.75	0.52	3.49
SDSS_J133737.49+155820.0	-0.4	-0.5	2.0	0.86	1.03
SDSS_J134159.72+294653.5	-0.2	0.1	2.0	1.15	2.33
SDSS_J135036.01+334217.3	-0.5	-0.3	1.75	0.76	2.33
SDSS_J135226.71+140528.5	-0.3	0.5	1.75	1.01	6.29
SDSS_J140528.32+304602.0	0.2	-0.1	1.75	0.98	5.27
SDSS_J141451.35+030751.2	0.1	0.5	2.0	3.01	6.24
SDSS_J141517.98-022641.0	-0.2	0.5	1.75	0.69	2.00
SDSS_J142724.23+372817.0	-0.1	-0.5	1.75	0.59	2.22
SDSS_J143156.59+164615.4	0.3	0.0	2.25	1.44	0.67
SDSS_J143312.96+525747.3	-0.1	-0.4	3.0	12.59	7.36
SDSS_J143424.79+024756.2	0.5	-0.1	1.75	0.87	2.60
SDSS_J143620.38+051951.5	-0.2	-0.5	1.75	1.18	8.18
SDSS_J144745.52+132032.2	-0.3	-0.2	2.25	3.38	2.72
SDSS_J145216.49+121711.5	-0.5	0.5	3.0	7.59	1.19
SDSS_J145243.25+165413.4	0.1	0.5	2.0	1.63	2.35

Table 3 continued on next page

Table 3 (*continued*)

Source Name	Right Ascension distance (°)	Declination distance (°)	Gamma Index (Γ)	Flux (10^{-9}) (ph cm $^{-2}$ s $^{-1}$)	Test Statistic
SDSS_J145616.20+203120.6	0.5	0.4	3.0	13.65	5.01
SDSS_J150152.30+174228.2	0.1	0.5	1.75	0.60	1.58
SDSS_J150425.68+074929.7	0.5	0.3	2.75	11.20	3.94
SDSS_J150601.89+084723.2	0.5	-0.4	3.0	20.71	5.73
SDSS_J150636.57+092618.3	0.5	-0.5	3.0	29.43	8.27
SDSS_J150808.25+265457.6	-0.4	-0.5	2.0	1.97	3.49
SDSS_J152010.94+254319.3	0.4	-0.4	1.75	0.36	1.61
SDSS_J152151.85+074231.7	-0.1	0.4	1.75	1.29	4.52
SDSS_J153016.15+270551.0	0.2	-0.1	1.75	0.61	2.66
SDSS_J154147.28+453321.7	0.5	-0.1	2.0	1.81	4.17
SDSS_J154426.93+470024.2	-0.3	-0.4	1.75	0.98	8.36
SDSS_J154451.23+433050.6	0.1	-0.5	2.25	0.45	0.08
SDSS_J155951.61+255626.3	0.5	0.5	3.0	11.39	3.46
SDSS_J155953.99+444232.4	-0.2	-0.4	1.75	0.73	6.63
SDSS_J160426.51+174431.1	-0.5	-0.5	1.75	0.33	1.17
SDSS_J160523.84+143851.6	0.0	-0.5	2.25	5.23	3.62
SDSS_J160616.02+181459.8	-0.1	0.0	1.75	0.41	2.44
SDSS_J160641.83+084436.8	0.2	0.4	1.75	1.01	3.30
SDSS_J161238.84+293836.9	0.1	0.1	2.25	3.07	2.56
SDSS_J161256.85+095201.5	0.2	0.4	2.0	2.99	4.21
SDSS_J162146.06+254914.4	0.4	-0.3	1.75	0.86	2.98
SDSS_J162549.96+402919.4	-0.5	0.3	2.0	2.08	3.89
SDSS_J162846.13+252940.9	0.2	0.3	3.0	9.42	2.42
SDSS_J162944.98+404841.6	-0.4	0.3	1.75	0.64	2.92
SDSS_J164925.86+360321.3	-0.3	0.5	1.75	0.66	2.79
SDSS_J165830.05+252324.9	-0.3	-0.2	2.25	4.97	4.00
SDSS_J170358.49+241039.5	-0.5	0.5	1.75	0.55	3.45
SDSS_J171522.97+572440.2	0.2	0.5	2.25	0.01	0.00
SDSS_J172215.41+304239.8	0.2	0.1	1.75	0.44	1.01

NOTE—Column description: (1) Source name; (2) (3) Distance added to the right ascension (declination) component of the source's position used in the fitting model; (4) Γ index of the power law which gave the maximum TS; (5) Flux upper limit (95% confidence level) corresponding to the maximum TS found in photons per centimeter square per second; (6) Maximum TS found for this source.

Search for gamma-ray counterparts of newly discovered radio astrophysical sources

Sergio Best
Asesor: Prof. José Bazo

March 18, 2019



PUCP

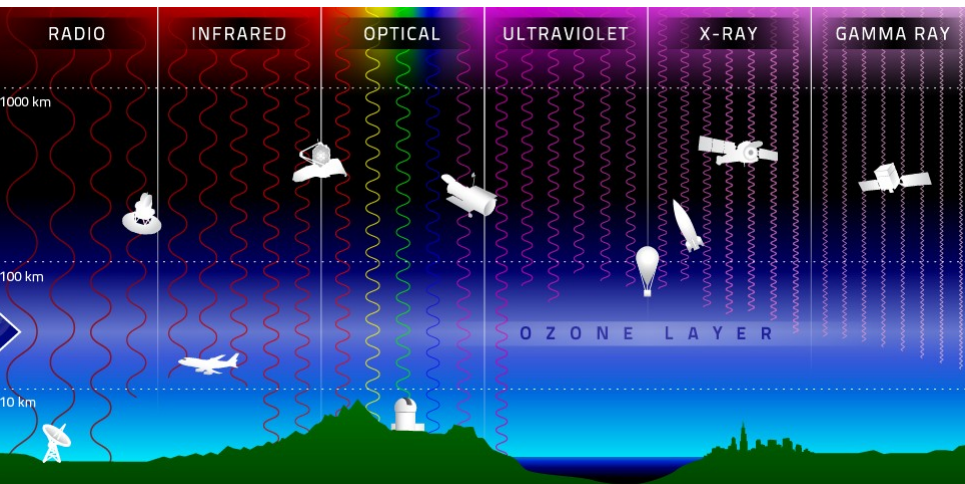


Tabla de contenidos

- **MOTIVACIÓN:** Presentaremos dos fuente de radio. FR0s y FRBs.
- **FERMI-LAT:** El detector de rayos gamma de donde sacamos los datos.
- **ESTADÍSTICA:** Breve introducción a lo que es el likelihood.
- **PROCEDIMIENTO:** Procedimiento de correlación.
- **RESULTADOS:** Algunas correlaciones encontradas.

Motivación

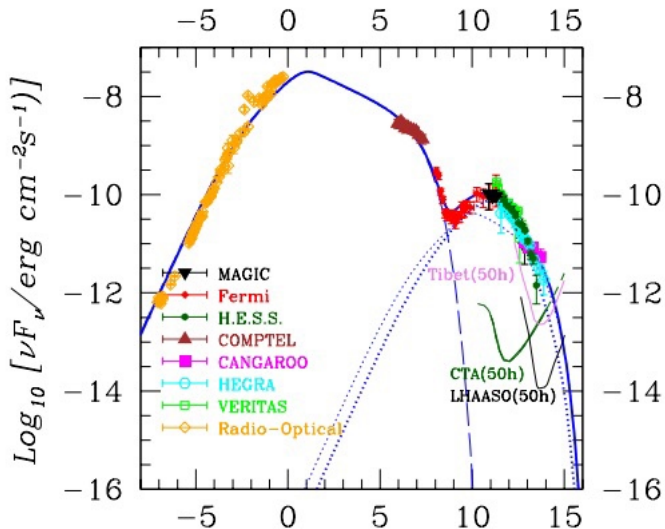
Espectro electromagnético



Fuente:

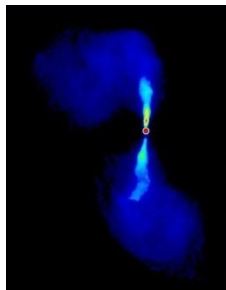
<http://ecuip.lib.uchicago.edu/multiwavelength-astronomy/astrophysics/07.html>

Crab Nebula

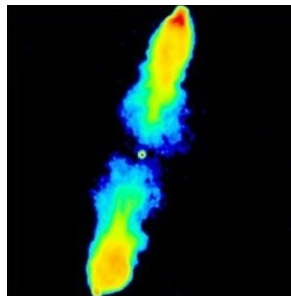


Clasificación Fanaroff-Riley:


FR-I: Luminosidad decrece como función de la distancia al centro.
Baja potencia.



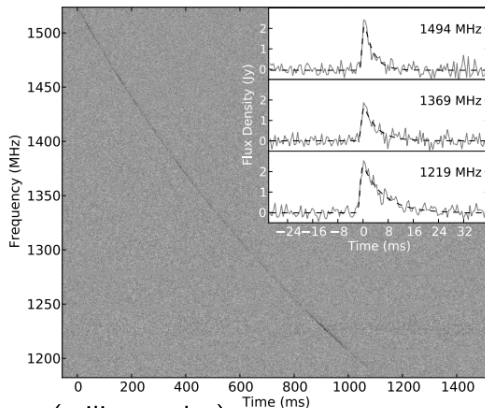
FR-II: Luminosidad se incrementa como función de la distancia al centro.
Alta potencia.



FR-0: Compacto ($<10\text{kpc}$), similar al FR-I pero sin estructuras extendidas.

Fuente: Active Galactic Nuclei with Fermi-LAT, Elisabetta Cavazzuti 

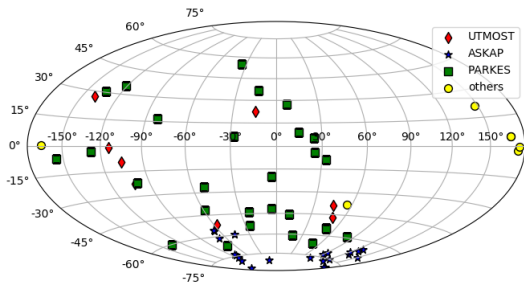
Fast Radio Bursts



- Cortos en tiempo (milisegundos).
- Rango de 1000 a 1500 MHz.
- Bastante energéticos.

<https://arxiv.org/abs/1307.1628>

Fast Radio Bursts



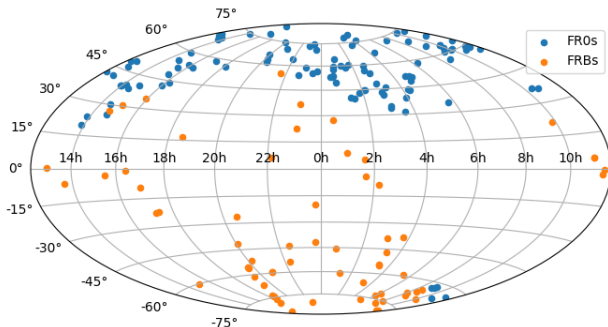
Origen desconocido, aunque probablemente extragalácticos debido a su distribución espacial y dispersion measure (DM).

$$DM = \int n_e dr \propto \Delta t \left(\frac{1}{\nu_2^2} - \frac{1}{\nu_1^2} \right)^{-1}$$

Coordenadas de FRBCat: <http://adsabs.harvard.edu/abs/2016PASA...33...45P>

Mapa de FR0s y FRBs

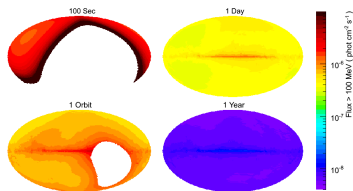
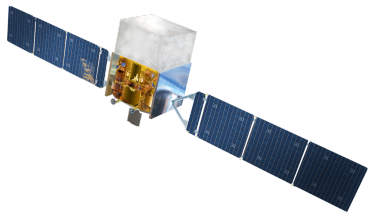
170 fuentes analizadas en total (62 FRBs y 108 FR0s).



Coordenadas de FR0-Cat: <https://arxiv.org/abs/1709.00015>

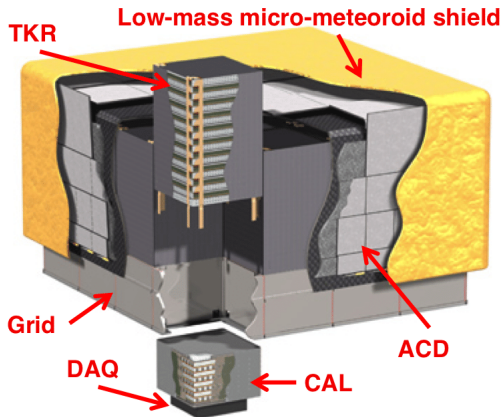
Coordenadas de FRBCat: <http://adsabs.harvard.edu/abs/2016PASA...33...45P>

Fermi-LAT



- **ÁREA:** 2.4 Sr \approx 20%
- **DETECCIÓN:** Rayos gamma
- **RANGO DE ENERGÍA:** 30 MeV - 300 GeV
- **RESOLUCIÓN:** \sim 1 arcminuto

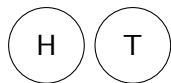
Principio de funcionamiento



- **VOLUMEN:** 1.8x1.8x0.72m
- **PROCESO:** $\gamma + X \rightarrow e^+e^- + X$

Likelihood

Lanzar monedas



p : probabilidad de obtener cara (0.5)

Lanzar monedas



p : probabilidad de obtener cara ($0.5 \rightarrow ?$)

Binomial



$$P(H, N, p) = \binom{N}{H} p^H (1 - p)^{N-H}$$

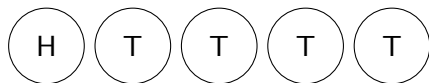
Binomial



$$P(H, N, p) = \binom{N}{H} p^H (1 - p)^{N-H}$$

$$p = 0.5 \rightarrow P(H, N) = \binom{N}{H} 0.5^N$$

Binomial



$$P(H, N, p) = \binom{N}{H} p^H (1-p)^{N-H}$$

$$p = 0.5 \rightarrow P(H, N) = \binom{N}{H} 0.5^N \rightarrow p = \binom{5}{1} 0.5^5 = 0.156$$

Binomial

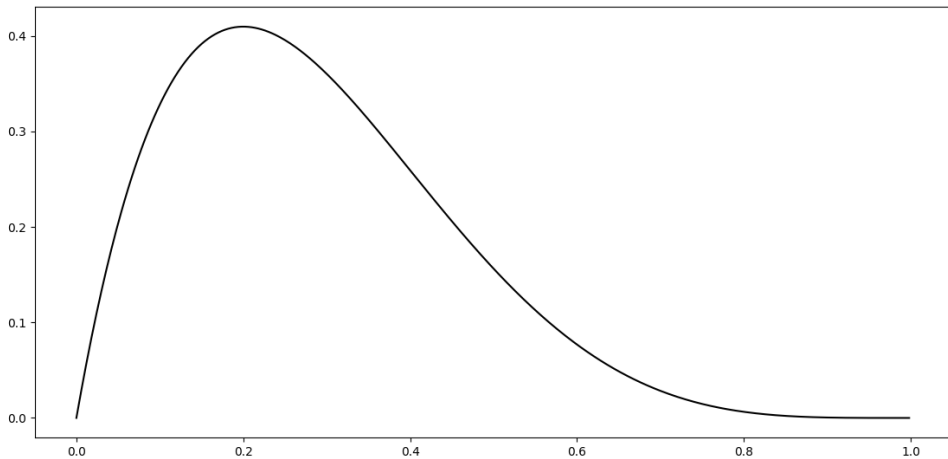


$$P(H, N, p) = \binom{N}{H} p^H (1-p)^{N-H}$$

$$p = 0.5 \rightarrow P(H, N) = \binom{N}{H} 0.5^N \rightarrow p = \binom{5}{1} 0.5^5 = 0.156$$

$$X = \{N = 5, H = 1\} \rightarrow \mathcal{L}(p) = \binom{5}{1} p^1 (1-p)^4 = 5p(1-p)^4$$

Likelihood



Maximum Likelihood Estimator

$$\mathcal{L}(\theta|x) = P_{\theta}(X = x)$$

Maximum Likelihood Estimator

$$\mathcal{L}(\theta|x) = P_{\theta}(X = x)$$

$$\theta_{ML} \equiv \max \mathcal{L}(\theta)$$

$$\left. \frac{\partial \mathcal{L}(\theta)}{\partial \theta} \right|_{\theta_{ML}} = 0$$

$$\left. \frac{\partial^2 \mathcal{L}(\theta)}{\partial \theta^2} \right|_{\theta_{ML}} < 0$$

Maximum Likelihood Estimator

$$\mathcal{L}(\theta|x) = P_{\theta}(X = x)$$

$$\theta_{ML} \equiv \max \mathcal{L}(\theta)$$

$$\left. \frac{\partial \mathcal{L}(\theta)}{\partial \theta} \right|_{\theta_{ML}} = 0$$

$$\left. \frac{\partial^2 \mathcal{L}(\theta)}{\partial \theta^2} \right|_{\theta_{ML}} < 0$$

Para nuestro ejemplo con monedas:

$$p_{ML} = \frac{1}{5} \quad \text{En general: } p_{ML} = \frac{H}{N}$$

Forma del Likelihood

$$\ln(\mathcal{L}(\theta)) =$$
$$\ln(\mathcal{L}(\theta_{ML})) + \frac{1}{\mathcal{L}(\theta)} \frac{\partial \mathcal{L}(\theta)}{\partial \theta} \Big|_{\theta_{ML}} (\theta - \theta_{ML}) + \frac{1}{2} \frac{\partial^2 \ln(\mathcal{L}(\theta))}{\partial \theta^2} \Big|_{\theta_{ML}} (\theta - \theta_{ML})^2$$

Forma del Likelihood

$$\ln(\mathcal{L}(\theta)) =$$

$$\ln(\mathcal{L}(\theta_{ML})) + \frac{1}{\mathcal{L}(\theta)} \frac{\partial \mathcal{L}(\theta)}{\partial \theta} \Big|_{\theta_{ML}} (\theta - \theta_{ML}) + \frac{1}{2} \frac{\partial^2 \ln(\mathcal{L}(\theta))}{\partial \theta^2} \Big|_{\theta_{ML}} (\theta - \theta_{ML})^2$$

$$\mathcal{L}(\theta) = \mathcal{L}(\theta_{ML}) \exp\left(-\frac{1}{2} \frac{(\theta - \theta_{ML})^2}{\Sigma_{\theta}^2}\right)$$

Forma del Likelihood

$$\ln(\mathcal{L}(\theta)) =$$

$$\ln(\mathcal{L}(\theta_{ML})) + \frac{1}{\mathcal{L}(\theta)} \frac{\partial \mathcal{L}(\theta)}{\partial \theta} \Big|_{\theta_{ML}} (\theta - \theta_{ML}) + \frac{1}{2} \frac{\partial^2 \ln(\mathcal{L}(\theta))}{\partial \theta^2} \Big|_{\theta_{ML}} (\theta - \theta_{ML})^2$$

$$\mathcal{L}(\theta) = \mathcal{L}(\theta_{ML}) \exp\left(-\frac{1}{2} \frac{(\theta - \theta_{ML})^2}{\Sigma_{\theta}^2}\right)$$

$$\mathcal{L}(\theta) \sim N(\theta_{ML}, \sqrt{\Sigma_{\theta}^2})$$

Log-Likelihood Ratio

$$TS = -2 \log \left(\frac{\mathcal{L}|\theta_0}{\mathcal{L}|\theta_{ML}} \right)$$

Log-Likelihood Ratio

$$TS = -2\log\left(\frac{\mathcal{L}|\theta_0}{\mathcal{L}|\theta_{ML}}\right) \sim \chi_{df=1}^2$$

Log-Likelihood Ratio

$$TS = -2\log\left(\frac{\mathcal{L}|\theta_0}{\mathcal{L}|\theta_{ML}}\right) \sim \chi_{df=1}^2$$

Ejemplo:

$$X = \{N = 100, H = 48\} \quad H_0 : p = \frac{1}{5}$$

Log-Likelihood Ratio

$$TS = -2 \log \left(\frac{\mathcal{L}|\theta_0}{\mathcal{L}|\theta_{ML}} \right) \sim \chi_{df=1}^2$$

Ejemplo:

$$X = \{N = 100, H = 48\} \quad H_0 : p = \frac{1}{5}$$

$$TS = 31.78 \rightarrow \sim 5.64\sigma$$

Procedimiento

LAT Photon, Event, and Spacecraft Data Query

Object name or coordinates:

Coordinate system:

Search radius (degrees):

Observation dates:

Time system:

Energy range (MeV):

LAT data type:

Spacecraft data:

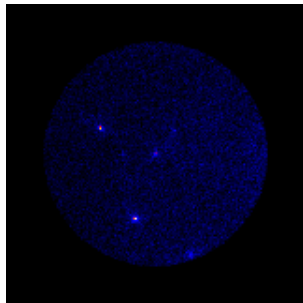
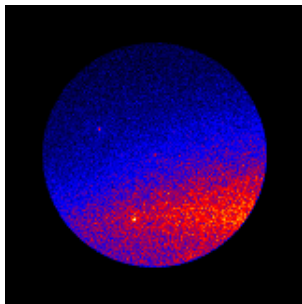
Start Search

Reset

<https://fermi.gsfc.nasa.gov/cgi-bin/ssc/LAT/LATDataQuery.cgi>

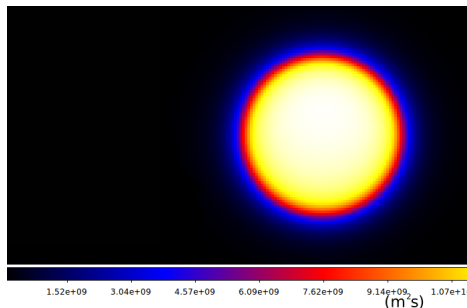
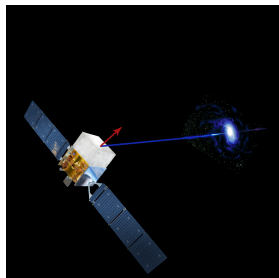
Filtrando fondo de la Tierra

Count maps.



Livetime Cube y Exposure Map

Respuesta del satelite al ángulo de inclinación y el tiempo de exposición.



Modelos

Power Law

$$\frac{dN}{dE} = N_0 \left(\frac{E}{E_0} \right)^{-\gamma}$$

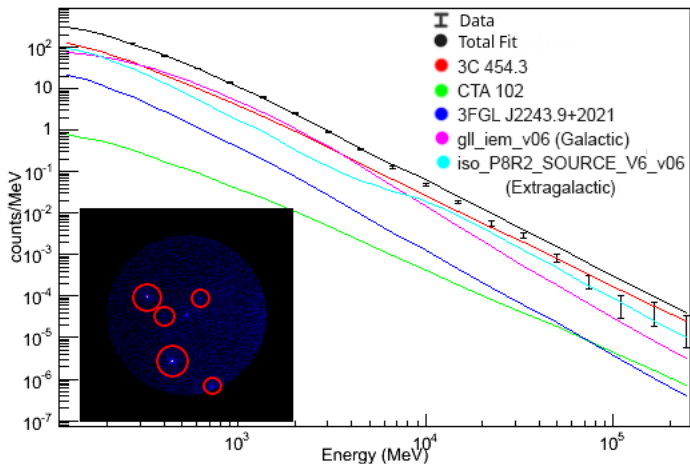
Log Parabola

$$\frac{dN}{dE} = N_0 \left(\frac{E}{E_b} \right)^{-(\alpha + \beta \log(\frac{E}{E_b}))}$$

Exponential Cutoff

$$\frac{dN}{dE} = N_0 \left(\frac{E}{E_0} \right)^{-\gamma_1} \exp\left(-\left(\frac{E}{E_c}\right)^{\gamma_2}\right)$$

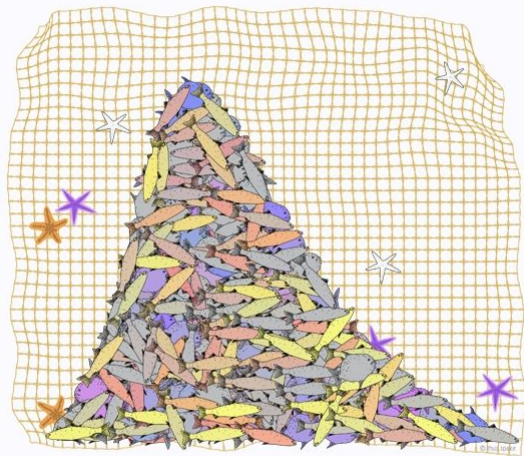
Se usaron funciones (e.g.: Power Law, Log Parabola) para modelar los fotones incidentes que correspondían a fuentes conocidas.



Binned Likelihood

$$p_i = \frac{m_i^{n_i} \exp[-m_i]}{n_i!}$$

$$\mathcal{L} = \exp[-N_{\text{exp}}] \prod_i \frac{m_i^{n_i}}{n_i!}$$

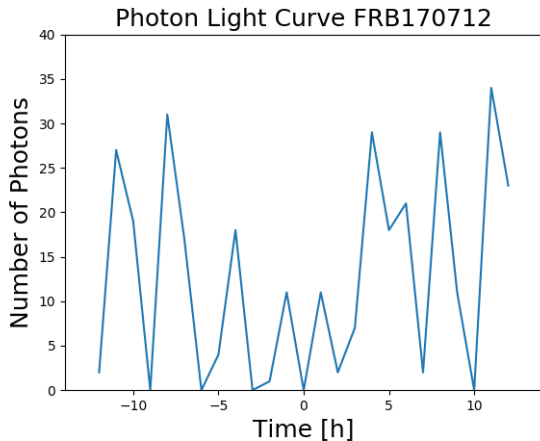


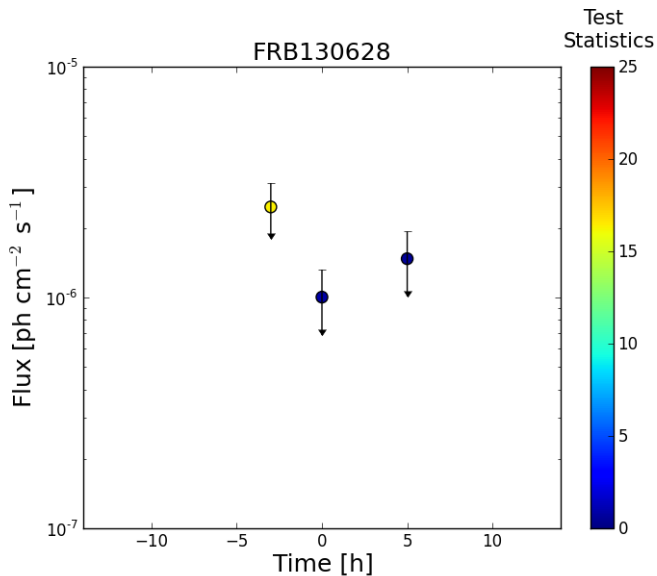
Análisis

- Agregamos un power law con parámetros fijos (Γ index = $\{1.75, 3.0\}$, $E_0 = 100$ MeV) excepto por N_0 para representar la fuente (FRB o FR0).
- Calculamos \mathcal{L} para $N_0 = 0$ lo que corresponde a la hipótesis nula (solo incluye fondo).
- Calculamos \mathcal{L} , el N_0 que dé el mayor likelihood posible.
- Finalmente calculamos el TS con estos dos likelihoods.

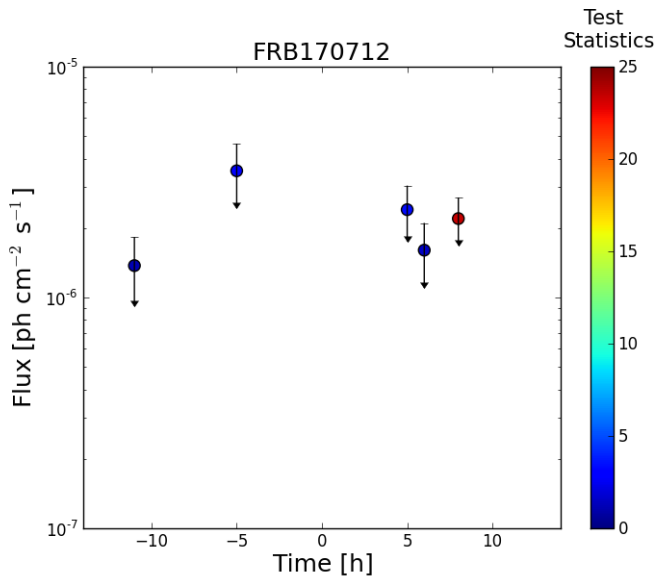
Resultados

Cuenta de Fotones

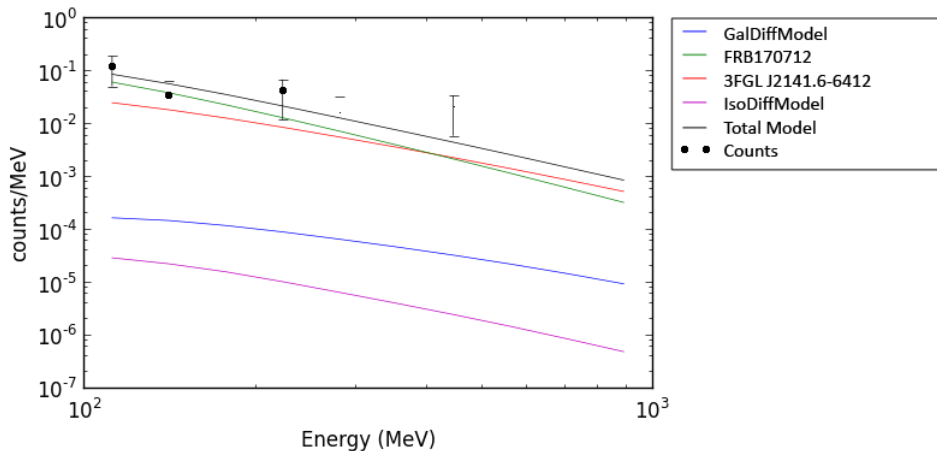




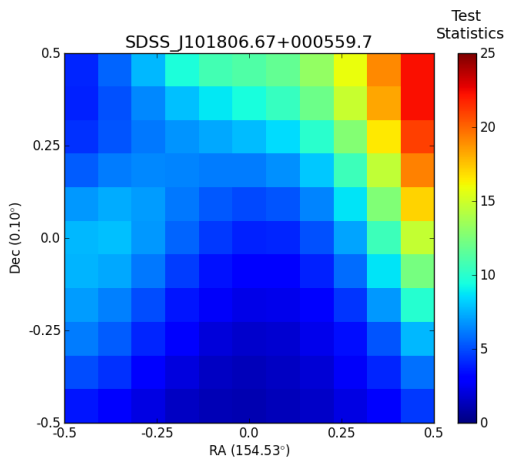
Lightcurve del FRB130628 mostrando upperlimits.



Lightcurve del FRB170712 mostrando upperlimits.

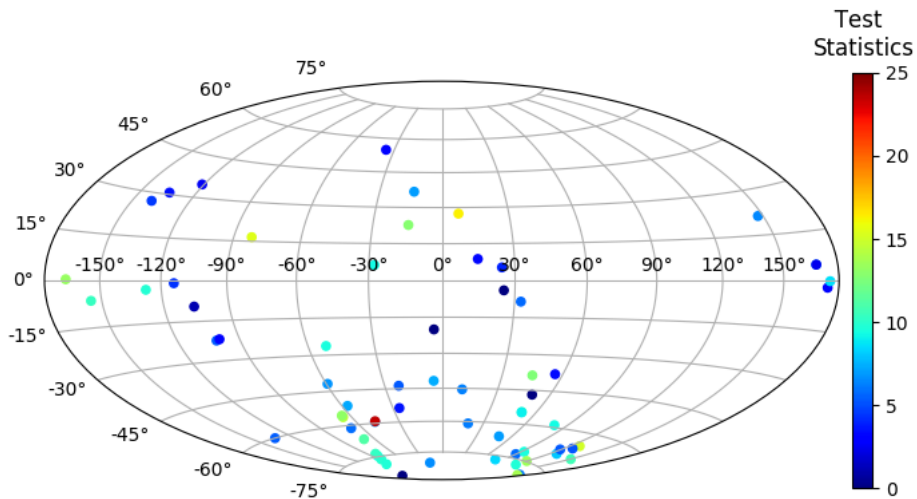


Spectral Energy Distribution del FRB170712 mostrando solo fuentes con $TS > 1$.

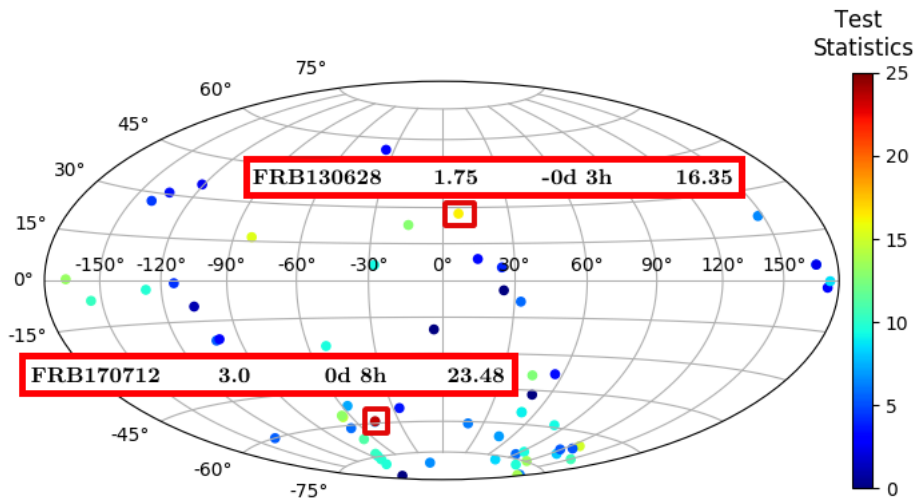


TSMaP de SDSS_J101806.67+000559.7. Cada pixel representa 0.1° . Los resultados corresponden al índice Γ que dio el máximo TS ($\Gamma = 2.5$).

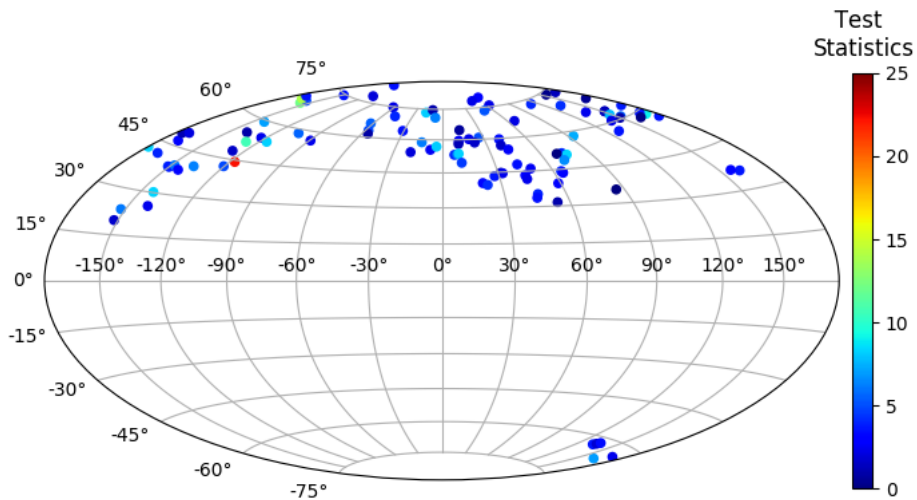
Mapa FRBs



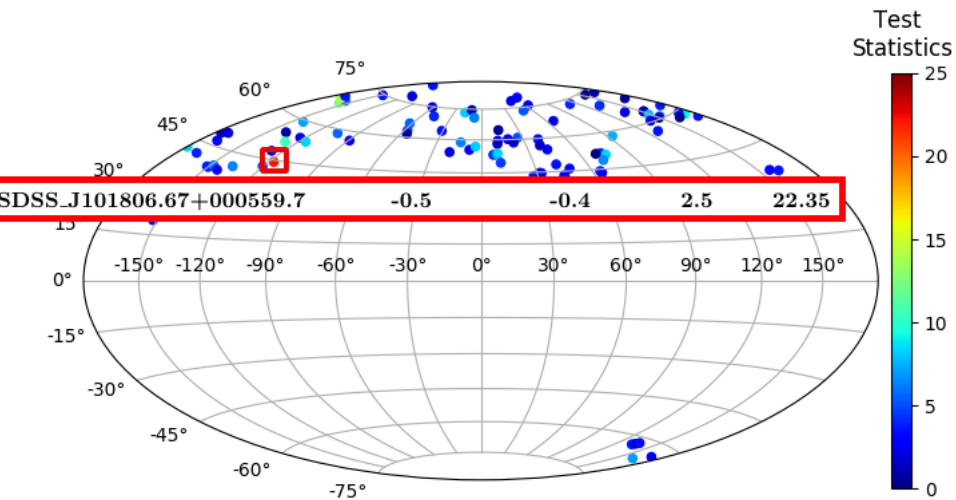
Mapa FRBs



Mapa FR0s



Mapa FR0s



Análisis adicionales

- **FRB130628:** Spectral energy distribution.
- **FRB170712:** Spectral energy distribution y lightcurve con exponential cutoff. (Nuevo TS Máximo de 23.75).
- **SDSS_J101806.67+000559.7:** TSMaP más amplio. TS bastante alto, orden de 60. Se debía a otra fuente cercana. Un blazar llamado 3FGL J1024.8+0105.

Resumen

- Empezamos con 170 fuentes de radio (entre FRBs y FR0s).
- Analizamos estas fuentes para encontrar correlaciones con rayos gamma usando el modelo de power law.
- Ninguna fuente tiene más de 5σ .
- De estas, tres fuentes tenían un TS que parecía indicar significancia en correlación ($> 4\sigma$).
- Por cercanía de otras fuentes, el único candidato con el que nos quedamos es el FRB170712.

Gracias

Bibliografía

- Atwood, W. B., Abdo, A. A., Ackermann, M., et al. 2009, , 697, 1071
- Baldi, R. D., Capetti, A., & Giovannini, G. 2015, AN, 337, Issue 1-2
- Baldi, R. D., Capetti, A., & Massaro, F. 2017, 609, A1
- Chatterjee, S., Law, C. J., Wharton, R. S., et al. 2017, , 337, 541, 58-61
- Deng, C. M., Cai, Y., Wu, X. F., Liang, E. W. 2018, , 98, 123016
- Fanaroff B. L., & Riley J. M., 1974, , 167, 31P
- Ginsburg, A., Astroquery 2019,
<https://astroquery.readthedocs.io/en/latest/>
- Grandi, P., Capetti, A., Baldi, R. D. 2015, , 457, 1
- Lorimer, D. R., Bailes, M., McLaughlin, M. A., Narkevic, D. J., & Crawford, F. 2007, Sci, 318, 5851

Margalit, B., Metzger, B. D., Berger, E., et al. 2018, , 481, 2

Osowski, S. 2018,

<http://www.astronomerstelegam.org/?read=11396>

Petroff, E., Barr, E. D., Jameson, A., et al. 2016, , 33, e045,

<http://frbcatalog.org>

Sanchez, D., Deil, C., Enrico 2013,

<https://enrico.readthedocs.io/en/latest/>

Scholz, P., Bogdanov, S., Hessels, J. W., et al. 2017, , 846, 1

Xi, S. Q., Tam, P. H. T., Peng, F. K., Wang, X. Y. 2017, , 842, 1